

Sunyaev-Zeldovich effects, free-free emission, and imprints on the cosmic microwave background

C. Burigana^a, G. De Zotti^b, L. Feretti^c

^aIASF/CNR-INAF, via Gobetti 101, I-40129 Bologna, Italy, *burigana@bo.iasf.cnr.it*

^bOAP/INAF, vicolo dell'Osservatorio 5, I-35122 Padova, Italy, *dezotti@pd.astro.it*

^cIRA/CNR-INAF, via Gobetti 101, I-40129 Bologna, Italy, *lferetti@ira.cnr.it*

The signatures from Sunyaev-Zeldovich effects and free-free emission in the intergalactic and intracluster medium and at galactic scales probe the structure evolution at various cosmic times. The detection of these sources and, possibly, the precise imaging of their spatial structure at the high resolution and sensitivity achievable with SKA will greatly contribute to the comprehension of crucial cosmological and astrophysical aspects, as the physical conditions of early ionized halos, quasars and proto-galactic gas and the mapping of the thermal and density structure of clusters of galaxies, with an extremely accurate control of extragalactic radio sources, which represents also a useful by-product for future CMB spectrum experiments devoted to probe the thermal plasma history at early times.

1. INTRODUCTION

The thermal plasma in the intergalactic and intracluster medium and at galactic scales leaves imprints on the cosmic microwave background (CMB) through the Thomson scattering of CMB photons on hot electrons and the free-free emission. Although not specifically devoted to CMB studies, because of its high resolution and the limited high frequency coverage, the extreme sensitivity and resolution of SKA may be fruitfully used for a detailed mapping of the above effects on dedicated sky areas. A particularly accurate control of the extragalactic radio sources represents a useful by-product for future CMB spectrum experiments devoted to probe the thermal plasma history at high redshifts. The SKA highest frequencies ($\simeq 20$ GHz) are, of course, the most advantageous to detect Sunyaev-Zeldovich effects on the CMB because of the steeper decrease of the synchrotron radio emission with the frequency.

2. THERMAL AND KINETIC SUNYAEV-ZELDOVICH EFFECT TOWARDS GALAXY CLUSTERS

The scattering of CMB photons from hot electrons in galaxies and clusters of galaxies produces a frequency dependent change in the CMB brightness. If the hot electron gas is globally at rest with respect to the observer only the thermal Sunyaev-Zeldovich (SZ) effect [51] (see also [42]) will be present; differently, a bulk peculiar motion, V_r , of the hot electron gas produces a kinetic SZ effect. In the Rayleigh-Jeans (RJ) region the first effect produces a decrement of the surface brightness, ΔI_{th} , towards the cluster. The second effect produces either a decrement or an increment, ΔI_k , depending on the direction of the cluster velocity with respect to the observer. Neglecting relativistic corrections:

$$\Delta I_{th} = I_0 y g(x) \quad (1)$$

and

$$\Delta I_k = -I_0 (V_r/c) \tau_e h(x), \quad (2)$$

where $I_0 = (2h_P/c^2)(k_B T_{CMB}/h)^3$. Here

$$\tau_e = \int n_e \sigma_T dl \quad (3)$$

and

$$y = \int (k_B T_e / m_e c^2) n_e \sigma_T dl \quad (4)$$

are respectively the Thomson optical depth and the Comptonization parameter [56] integrated over the cluster along the line of sight, n_e being the electron density, and

$$h(x) = x^4 e^x / (e^x - 1)^2 \quad (5)$$

$$g(x) = h(x)[x(e^x + 1)/(e^x - 1) - 4], \quad (6)$$

where $x = h_P \nu / k_B T_{CMB}$ is a dimensionless photon frequency. The two effects have a different frequency dependence that in principle allows their separation through multi-frequency observations. SKA observations in the RJ regime (where $h(x) \sim g(x) \rightarrow x^2$) can be combined with millimetric observations (in particular $g(x) \simeq 0$ and $h(x)$ is maximum at ~ 217 GHz).

Many thousands of galaxy clusters will be identified by XMM ($\sim 10^3$), Planck ($\sim 10^4$), and SDSS ($\sim 5 \times 10^5$). The typical angular sizes of galaxy clusters range from \sim arcmin to few tens of arcmin.

The SKA sensitivity and resolution mainly depends on the used array collecting area. By considering a frequency band of $\simeq 4$ GHz at 20 GHz, the whole instrument collecting area will allow to reach a (rms) sensitivity of $\simeq 40$ nJy in one hour of integration with an angular resolution of $\simeq 1$ mas (considering $\simeq 3000$ km maximum baseline). By using only about 50% of the collecting area within $\simeq 5$ km, the (rms) sensitivity in one hour of integration is $\simeq 80$ nJy with a resolution of $\simeq 0.6''$.

Although the major role on the study of the SZ effects towards galaxy clusters will be played by dedicated telescopes operating at \simeq arcmin resolutions with frequency coverages up to \simeq millimetric wavelengths [20], with the 50% of the SKA collecting area it will be possible to accurately map the SZ effect [49] of each considered cluster, particularly at moderately high redshifts, with

an extremely precise subtraction of discrete radio sources (see also Sect. 4). The combination with X-ray images, in particular with those expected by the wide field imager (WFI) on board the X-ray Evolving Universe Spectroscopy (XEUS) satellite ¹ by ESA designed to reach a resolution of $0.25''$ on a FOV of $5' - 10'$, will allow to accurately map the thermal and density structure of the gas in galaxy clusters.

Finally, we note that it is also possible to study the SZ effect (both thermal and kinetic) from clusters in a statistical sense, namely through its contribution to the angular power spectrum, C_ℓ , (see Appendix A) of the CMB secondary anisotropies. This topic has been investigated in several papers (see, e.g., [35,54,15,45,11,26]). At sub-arcmin scales (i.e. at multipoles $\ell \gtrsim 10^4$) secondary anisotropies from thermal (more important at $\ell \lesssim \text{few} \times 10^4$) and kinetic (more important at $\ell \gtrsim \text{few} \times 10^4$) SZ effect dominate over CMB primary anisotropy whose power significantly decreases at multipoles $\ell \gtrsim 10^3$ because of photon diffusion (Silk damping effect [47]). Their angular power spectrum at $\ell \sim 10^4 - 10^5$ ($\approx 10^{-12} - 10^{-13}$ in terms of dimensionless $C_\ell \ell(2\ell+1)/4\pi$) could be in principle investigated with the sensitivity achievable with SKA (see Fig. 6 and Appendix A). On the other hand, at the SKA resolution and sensitivity the contribution to fluctuations from foreground sources (both diffuse radio emission, SZ effects, and free-free emitters) at galaxy scales probably dominates over the SZ effect from clusters.

3. THERMAL SUNYAEV-ZELDOVICH EFFECT AT GALAXY SCALE

The proto-galactic gas is expected to have a large thermal energy content, leading to a detectable SZ signal, both when the protogalaxy collapses with the gas shock-heated to the virial temperature [41,55], and in a later phase as the result of strong feedback from a flaring active nucleus (see, e.g., [19,30,31,1,38,21]). The astrophysical implications of these scenarios have been recently investigated by [10].

¹<http://sci.esa.int/science-e/www/area/index.cfm?fareaid=25>

A fully ionized gas with a thermal energy density ϵ_{gas} within the virial radius

$$\begin{aligned} R_{\text{vir}} &= \left(\frac{3M_{\text{vir}}}{4\pi\rho_{\text{vir}}} \right)^{1/3} & (7) \\ &\simeq 1.6 \cdot 10^2 h^{-2/3} (1+z_{\text{vir}})^{-1} \\ &\quad \left(\frac{M_{\text{vir}}}{10^{12}M_{\odot}} \right)^{1/3} \text{kpc}, \end{aligned}$$

transfers to the CMB an amount $\Delta\epsilon \simeq (\epsilon_{\text{gas}}/t_c)2(R_{\text{vir}}/c)$ of thermal energy through Thomson scattering producing a Comptonization parameter [56] $y \simeq (1/4)\Delta\epsilon/\epsilon_{\text{CMB}}$. Here h is the Hubble constant in units of $100 \text{ km s}^{-1} \text{ Mpc}^{-1}$ and $\rho_{\text{vir}} \simeq 200\rho_u$, $\rho_u = 1.88 \times 10^{-29}h^2(1+z_{\text{vir}})^3 \text{ g cm}^{-3}$ is the mean density of the universe at the virialization redshift z_{vir} ; $\epsilon_{\text{CMB}} = a_{BB}T_{\text{CMB}}^4 \simeq 4.2 \times 10^{-13}(1+z)^4 \text{ erg cm}^{-3}$, a_{BB} being the black-body constant and $T_{\text{CMB}} = T_0(1+z)$ the temperature of the CMB; t_c is the gas cooling time by Thomson scattering.

Assuming the binding energy ($E_{\text{b,gas}} = M_{\text{gas}}v_{\text{vir}}^2$, $v_{\text{vir}} = 162h^{1/3}(1+z)^{1/2}(M_{\text{vir}}/10^{12}M_{\odot})^{1/3} \text{ km s}^{-1}$ being the circular velocity of the galaxy at its virial radius [32,4]) to characterize the thermal energy content of the gas, E_{gas} , the amplitude of the SZ dip in the RJ region can be written as:

$$\begin{aligned} |\Delta T|_{\text{RJ}} &= 2yT_{\text{CMB}} & (8) \\ &\simeq 1.7 \left(\frac{h}{0.5} \right)^2 \left(\frac{1+z_{\text{vir}}}{3.5} \right)^3 \\ &\quad \frac{M_{\text{gas}}/M_{\text{vir}}}{0.1} \frac{M_{\text{vir}}}{10^{12}M_{\odot}} \frac{E_{\text{gas}}}{E_{\text{b,gas}}} \mu\text{K}. \end{aligned}$$

This SZ effect shows up on small (typically subarcmin) angular scales.

Quasar-driven blast-waves could inject into the ISM an amount of energy several times higher than the gas binding energy, thus producing larger, if much rarer, SZ signals. A black-hole (BH) accreting a mass M_{BH} with a mass to radiation conversion efficiency ϵ_{BH} releases an energy $E_{\text{BH}} = \epsilon_{\text{BH}}M_{\text{BH}}c^2$. We adopt the standard value for the efficiency $\epsilon_{\text{BH}} = 0.1$ and assume that a fraction $f_h = 0.1$ of the energy is fed in kinetic form and generates strong shocks turning it into heat.

Using the recent re-assessment by [53] of the well known correlation between the BH mass and the stellar velocity dispersion, $M_{\text{BH}} = 1.4 \times 10^8 (\sigma/200 \text{ km/s})^4 M_{\odot}$, we get

$$\begin{aligned} \frac{E_{\text{BH}}}{E_{\text{b,gas}}} &\simeq 4.7 \left(\frac{h}{0.5} \right)^{-2/3} \frac{\epsilon_{\text{BH}}}{0.1} \frac{f_h}{0.1} \frac{1+z_{\text{vir}}}{3.5} & (9) \\ &\quad \left(\frac{M_{\text{gas}}/M_{\text{vir}}}{0.1} \right)^{-1} \left(\frac{M_{\text{vir}}}{10^{12}M_{\odot}} \right)^{-1/3}. \end{aligned}$$

The amplitude of the SZ dip in the RJ region due to quasar heating of the gas is then estimated as:

$$\begin{aligned} \left| \left(\frac{\Delta T}{T} \right)_{\text{RJ}} \right| &\simeq 1.8 \times 10^{-5} \frac{f_h}{0.1} & (10) \\ &\quad \left(\frac{h}{0.5} \right)^2 \left(\frac{\epsilon_{\text{BH}}}{0.1} \right)^{1/2} \left(\frac{E_{\text{BH}}}{10^{62}} \right)^{1/2} \left(\frac{1+z}{3.5} \right)^3. \end{aligned}$$

Following [38], we adopt an isothermal density profile of the galaxy. The virial radius, encompassing a mean density of $200\rho_u$, is then:

$$\begin{aligned} R_{\text{vir}} &\simeq 120 \left(\frac{h}{0.5} \right)^{-1} \left(\frac{E_{\text{BH}}}{10^{62}} \right)^{1/4} & (11) \\ &\quad \left(\frac{\epsilon_{\text{BH}}}{0.1} \right)^{-1/4} \left(\frac{1+z_{\text{vir}}}{3.5} \right)^{-3/2} \text{kpc}, \end{aligned}$$

corresponding to an angular radius:

$$\begin{aligned} \theta_{\text{SZ}} &\simeq 17'' \left(\frac{E_{\text{BH}}}{10^{62}} \right)^{1/4} \left(\frac{\epsilon_{\text{BH}}}{0.1} \right)^{-1/4} & (12) \\ &\quad \left(\frac{1+z_{\text{vir}}}{3.5} \right)^{-3/2} \frac{d_A(2.5)}{d_A(z)}, \end{aligned}$$

where $d_A(z)$ is the angular diameter distance.

The angular scales of these SZ signals from galaxies are of the order of $\approx 10''$, then of particular interest for a detailed mapping with the SKA and XEUS in the radio and X-ray, respectively. The probability of observing these SZ sources on a given sky field at a certain flux detection level and the corresponding fluctuations are mainly determined by the redshift dependent source number density $\phi_{\text{SZ}}(S_{\text{SZ}}, z)$ per unit interval of the SZ (decrement) flux S_{SZ} . The lifetime of the considered SZ sources is crucial to determine their number density.

For quasar-driven blast-waves the lifetime of the active phase, t_{SZ} , is approximately equal

to the time for the shock to reach the outer boundary of the host galaxy. Assuming a self-similar blast-wave expanding in a medium with an isothermal density profile, $\rho \propto r^{-2}$, we have:

$$t_{\text{SZ}} \simeq 1.5 \times 10^8 \left(\frac{h}{0.5} \right)^{-3/2} \left(\frac{E_{\text{BH}}}{10^{62} \text{erg}} \right)^{1/8} \left(\frac{\epsilon_{\text{BH}}}{0.1} \right)^{-5/8} \left(\frac{f_h}{0.1} \right)^{-1/2} \left(\frac{1+z}{3.5} \right)^{-9/4} \text{yr.} \quad (13)$$

The evolving B-band luminosity function of quasars, $\phi(L_B, z)$, can be then adopted to derive the source number density $\phi_{\text{SZ}}(S_{\text{SZ}}, z)$ according to

$$\phi_{\text{SZ}}(S_{\text{SZ}}, z) = \phi(L_B, z) \frac{t_{\text{SZ}}}{t_{\text{q, opt}}} \frac{dL_B}{dS_{\text{SZ}}}, \quad (14)$$

where $L_B(S_{\text{SZ}}, z)$ is the blue luminosity of a quasar at redshift z causing a (negative) SZ flux S_{SZ} , and $t_{\text{q, opt}}$ is the duration of the optically bright phase of the quasar evolution.

For the proto-galactic gas t_{SZ} should be replaced by the gas cooling time, t_{cool} . Assuming that quasars can be used as effective signposts for massive spheroidal galaxies in their early evolutionary phases [16] and that they emit at the Eddington limit and using the relation by [12] between the mass of the dark-matter halo, M_{vir} , and the mass of the central black-hole, $M_{\text{BH}}/10^8 M_{\odot} \sim 0.1(M_{\text{vir}}/10^{12} M_{\odot})^{1.65}$, the number density of sources with gas at virial temperature can be straightforwardly related to the quasar luminosity function $\phi(L_B, z)$.

In spite of the many uncertainties of these models, it is remarkable that the CMB fluctuations (dominated at small scales by the Poisson contribution) induced by the SZ effect of these source populations could contribute to the CBI anisotropy measure and, in particular, could explain the angular power spectrum (see also Appendix A) found by BIMA at multipoles $\ell \approx (4 - 10) \times 10^3$ (see Fig. 1).

A direct probe of these models and, possibly, their accurate knowledge through a precise high resolution imaging is then of particular interest. Fig. 2 shows the number counts at 20 GHz predicted by these models: in a single SKA FOV about few $\times 10^2 - 10^3$ SZ sources with fluxes above

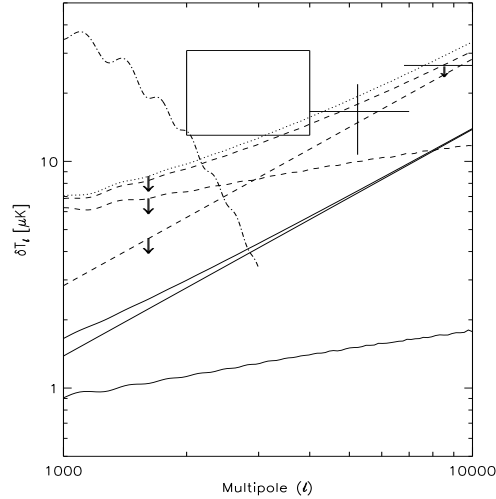


Figure 1. Angular power spectrum of SZ effects at 30 GHz compared to CMB primary fluctuation power spectrum and CBI [27] (box) and BIMA [9] (data points) measures. Solid lines represent clustering (bottom line), Poisson (middle line) and global (upper line) contributions from quasar driven blast-waves. Dashed lines represent clustering (bottom line at high ℓ), Poisson (middle line at high ℓ) and global (upper line) contributions from proto-galactic gas. The latter are actually upper limits since, because of the uncertainty in the cooling time, the extreme assumption that $t_{\text{cool}} = t_{\text{exp}}$ has been adopted in the computation. Dots refer to the overall contribution.

~ 100 nJy could be then observed in few hours of integration. Given the typical source sizes, we expect a blend of sources in the SKA FOV at these sensitivity levels, while much shorter integration times, \sim sec, on many FOV would allow to obtain much larger maps with a significant smaller number of resolved SZ sources per FOV. Both surveys on relatively wide sky areas and deep exposures on limited numbers of FOV are interesting and easily obtainable with SKA.

A different scenario to jointly explain the power excess found by BIMA and the high redshift

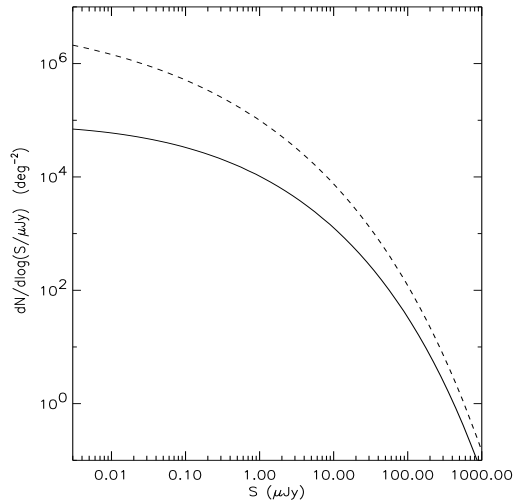


Figure 2. Number count predictions at 20 GHz for SZ effects as function of the absolute value of the flux from proto-galactic gas heated at the virial temperature (dashes) assuming $M_{\text{gas}}/M_{\text{vir}} = 0.1$ and from quasar driven blast-waves (solid line). The exponential model for the evolving luminosity function of quasars is derived by [37] for an optical spectral index of quasars $\alpha = 0.5$ ($S_\nu \propto \nu^\alpha$). The parameters have been set at $\epsilon_{\text{BH}} = 0.1$, $f_h = 0.1$, $k_{\text{bol}} = 10$, $t_{\text{q, opt}} = 10^7$ yr.

reionization detected by WMAP [25] ($z_{\text{reion}} \sim 15 - 20$) has been proposed by [34]. It involves hot gas winds powered by pair-instability supernovae (SN) explosions from the first generation of very massive stars at very low metallicity able to photoevaporate the gas in the halo potential. The SN remnants should then dissipate their energy in the intergalactic medium (IGM) and about 30–100% of their energy would be transferred to the CMB via Compton cooling. The resulting SZ effect from this sources is relevant in statistical sense. It is claimed to explain the high ℓ BIMA excess of the CMB angular power spectrum and to be able to generate a global Comptonization distortion parameter $y \sim \text{few} \times 10^{-6}$. However, it is estimated to be too faint ($\approx \text{few} \times 10^{-2}$ nJy)

to be observable even by SKA.

4. SKA CONTRIBUTION TO FUTURE CMB SPECTRUM EXPERIMENTS

The current limits on CMB spectral distortions and the constraints on energy dissipation processes $|\Delta\epsilon/\epsilon_i| \lesssim 10^{-4}$ in the plasma [44] are mainly set by COBE/FIRAS [28,13]. CMB spectrum experiments from space, DIMES [23] (see also [24]) at $\lambda \gtrsim 1$ cm and FIRAS II [14] at $\lambda \lesssim 1$ cm, have been proposed with an accuracy potentially able to constrain (or probably detect) energy exchanges 10–100 times smaller than the FIRAS upper limits. In particular, experiments like DIMES may probe dissipation processes at early times ($z \gtrsim 10^5$) resulting in Bose-Einstein like distortions [50,8,5] and free-free distortions [2] possibly generated by heating (but, although disfavoured by WMAP, in principle also by cooling [48]) mechanisms at late epochs ($z \lesssim 10^4$), before or after the recombination era [7]. The high redshift reionization detected by WMAP [25] supports the existence of late coupled Comptonization (with $\Delta\epsilon/\epsilon_i \simeq 4y \approx \text{few} \times 10^{-6}$, ϵ_i being the CMB energy density before the beginning of the dissipation process) and free-free distortions (with a highly model dependent amplitude) [6]. Typical distorted spectra potentially detectable by DIMES are shown in Fig. 3. To firmly observe such small distortions the Galactic and extragalactic foreground contribution should be accurately modelled and subtracted.

Recent progress on radio source counts at 1.4 GHz have been presented in [39]. On the other hand, the very faint tail of radio source counts is essentially unexplored and their contribution to the radio background at very low brightness temperature is not accurately known. For illustration, by assuming differential source number counts, $N(S)$, given by $\log N(S)/\Delta N_0 \sim a \log S + b$, with $\Delta N_0 \sim 150 S^{-2.5} \text{ sr}^{-1} \text{ Jy}^{-1}$ (S in Jy) [52], for $a \sim 0.4 - 0.6$ and $b \sim -(0.5 - 1)$, we find a contribution to the radio background at 5 GHz from sources between ~ 1 nJy and $\sim 1\mu\text{Jy}$ between few tens of μK and few mK. These signals are clearly negligible compared to

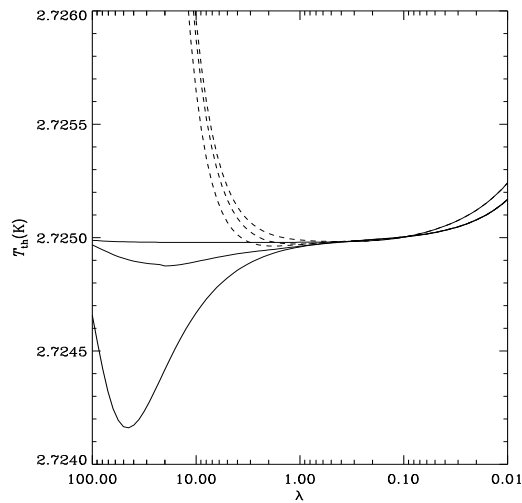


Figure 3. CMB distorted spectra as functions of the wavelength λ (in cm) in the presence of a late energy injection with $\Delta\epsilon/\epsilon_i = 5 \times 10^{-6}$ plus an early/intermediate energy injection with $\Delta\epsilon/\epsilon_i = 5 \times 10^{-6}$ occurring at the “time” Comptonization parameter $y_h = 5, 1, 0.01$ (from the bottom to the top; in the figure the cases at $y_h = 5$ and 1 are indistinguishable at short wavelengths; solid lines) and plus a free-free distortion with $y_B = 10^{-6}$ (dashes). y_h is defined by Eq. (4) with $dl = cdt$ and $T_e = T_{CMB}$ when the integral is computed from the time of the energy injection to the current time.

the accuracy of current CMB spectrum experiments, in particular at $\lambda \gtrsim 1$ cm, but are significant at the accuracy level on CMB distortion parameters potentially achievable with experiments like DIMES. This effect is small compared to the Galactic radio emission, whose accurate knowledge currently represents the major astrophysical problem in CMB spectrum experiments, but, differently from Galactic emission, it is isotropic at the angular scales of few degrees and can not be then subtracted from the CMB monopole temperature on the basis of its angular correlation properties. With accurate absolute measures on a

wide frequency coverage a fit including both CMB distorted spectra and astrophysical contributions can be searched (see [44] for an application to FIRAS data) but a direct radio background estimate from precise number counts will certainly improve the robustness of this kind of analyses.

The SKA sensitivity at 20 GHz will allow the detection (to 5σ) of sources down to a flux level of $\simeq 200$ nJy ($\simeq 60, 20, 6$ nJy) in 1 ($10, 10^2, 10^3$) hour(s) of integration over the $\simeq 1$ mas (FWHM) resolution element; similar numbers (from $\simeq 250$ to 8 nJy in an integration time from 1 to 10^3 hours, respectively) but on a resolution element about 10 times larger will be reached at \approx GHz frequencies by using a frequency bandwidth of about 25%.

Therefore, the SKA accurate determination of source number counts down to very faint fluxes can directly help the solution of one fundamental problem of the future generation of CMB spectrum space experiments at $\lambda \gtrsim 1$ cm.

5. FREE-FREE EMITTERS

The epoch of reionization has been extensively studied in the recent years and in particular since the WMAP 1-yr data release. Reionization affects the CMB both in anisotropies at large and small scales and in the spectrum. The understanding of the ionizing emissivity of collapsed objects and the degree of gas clumping is crucial for reionization models. The observation of diffuse gas and Population III objects in thermal bremsstrahlung as a direct probe of these quantities has been investigated by [33]. Free-free emission produces both global and localized spectral distortion of the CMB. A natural way to distinguish between free-free distortion by ionized halos rather than by diffuse ionized IGM is represented by observations at high resolution of dedicated sky areas and by the fluctuations in the free-free background. In the model by [33] halos collapse and form a starburst lasting $t_o = 10^7$ yr, then recombine and no longer contribute to the free-free background. By adopting a Press-Schechter model [40,3] for the number density of collapsed halos per mass interval, dn_{PS}/dM , [33] exploited the expression by [46] for the collapse rate of halos

per mass interval per unit comoving volume:

$$\frac{d\dot{N}^{form}}{dM}(M, z) = \frac{1}{D} \frac{dD}{dt} \frac{dn_{PS}}{dM}(M, z) \frac{\delta_c^2}{\sigma^2(M)D^2}; \quad (15)$$

here $D(z)$ is the growth factor and $\delta_c = 1.7$ is the threshold above which mass fluctuations collapse. The expected comoving number density of ionized halos in a given flux interval as a function of redshift

$$\frac{dN_{\text{halo}}}{dSdV}(S, z) = \int_{t(z)}^{t(z)-t_o} dt \frac{d\dot{N}^{form}}{dM} \frac{dM}{dS} \quad (16)$$

can be then computed given the expected flux from a halo of mass M at redshift z , $S = S(M, z)$, and the starburst duration, t_o . Adopting a cut-off mass for a halo to be ionized of $M_* = 10^8(1 + z/10)^{-3/2}M_\odot$ (the critical mass needed to attain a virial temperature of 10^4 K to excite atomic hydrogen cooling), [33] computed the number counts of sources above the flux limit S_c from the zeroth moment of the intensity distribution moments due to sources above a redshift z_{\min} ,

$$\begin{aligned} & \langle S^n (> z_{\min}, S_c) \rangle \quad (17) \\ & = \int_{z_{\min}}^{\infty} dz \int_{S_{\min}(z)}^{S_{\max}} dS \frac{dN_{\text{halo}}}{dSdV} \frac{dV}{dzd\Omega} S^n, \end{aligned}$$

by setting $S_{\max} \rightarrow \infty$ and $S_{\min}(z) = \max(S_c, S_*(z))$, where $S_*(z)$ denotes the flux from a halo of minimum mass M_* at redshift z .

The relation $\dot{N}_{\text{recomb}} = \alpha_B \langle n_e^2 \rangle V \approx (1 - f_{\text{esc}}) \dot{N}_{\text{ion}}$, between the production rate of recombination line photons, \dot{N}_{recomb} , and the production rate of ionizing photons, \dot{N}_{ion} , (here α_B is the recombination coefficient and f_{esc} (\approx some%) is the escape fraction for ionizing photons) implies that the source luminosities in H α and free-free emission ($\propto n_e^2 V$) are proportional to the production rate of ionizing photons. Over a wide range of nebulosity conditions [18] found that $\simeq 0.45$ H α photons are emitted per Lyman continuum photon; thus $L(\text{H}\alpha) = 1.4 \times 10^{41} \dot{N}_{\text{ion}} / (10^{53} \text{ ph s}^{-1}) \text{ erg s}^{-1}$. Given the free-free volume emissivity [43] in the case of an approximate mild temperature dependence with a power law (a velocity averaged Gaunt factor $\bar{g}_{ff} = 4.7$ is assumed), $\epsilon_\nu = 3.2 \times$

$10^{-39} n_e^2 (T/10^4 \text{ K})^{-0.35} \text{ erg s}^{-1} \text{ cm}^{-3} \text{ Hz}^{-1}$, it is found

$$L_\nu^{ff} = 1.2 \times 10^{27} \frac{\dot{N}_{\text{ion}}}{10^{53} \text{ ph s}^{-1}} \text{ erg s}^{-1} \text{ Hz}^{-1}. \quad (18)$$

Assuming the starburst model of [17] normalised to the observed metallicity $10^{-3} Z_\odot \leq Z \leq 10^{-2} Z_\odot$ of the IGM at $z \sim 3$ (resulting into a constant fraction of the gas mass turning into stars, $1.7\% \leq f_{\text{star}} \leq 17\%$, in a starburst which fades after $\sim 10^7$ yr), [33] derived a production rate of ionizing photons as a function of halo mass given by:

$$\dot{N}_{\text{ion}}(M) = 2 \times 10^{53} \frac{f_{\text{star}}}{0.17} \frac{M}{10^9 M_\odot} \text{ ph s}^{-1}, \quad (19)$$

which specifies the above free-free ionized halo luminosity. The corresponding flux is then:

$$\begin{aligned} & L_{\text{ff}} = \frac{L_\nu^{ff}}{4\pi d_L^2} (1+z) \quad (20) \\ & \approx 2.5 \left(\frac{1+z}{10} \right)^{-1} \frac{M}{10^9 M_\odot} \left(\frac{T}{10^4 \text{ K}} \right)^{-0.35} \text{ nJy}. \end{aligned}$$

Clearly, SKA will allow to detect only bright sources with deep exposures. The ionized halo number counts can be calculated from Eq. (17). The result by [33] is reported in Fig. 4: SKA should be able to detect $\sim 10^4$ individual free-free emission sources with $z > 5$ in 1 square degree above a source detection threshold of 70 nJy. The redshift information from the Balmer line emission detectable by the Next Generation Space Telescope (NGST) can be used to discriminate ionized halos from other classes of radio sources.

Ionized halos may contribute to the temperature fluctuations. In particular, the Poisson contribution is predicted to be larger (smaller) than the clustering one at scales smaller (larger) than $\sim 30''$ [33]. On the other hand, both are likely dominated by the radio source contribution.

Finally, the integrated emission from ionized halos produces a global CMB spectral distortion, $\Delta T_{ff} = c^2 \langle S \rangle / 2k_B \nu^2$, that can be computed from the mean sky averaged signal $\langle S \rangle$. By using Eq. (17) (since no point source removal is feasible at degree scales) with z_{\min} and $S_c = 0$, [33] found a free-free distortion $\Delta T_{ff} = 3.4 \times 10^{-3} \text{ K}$

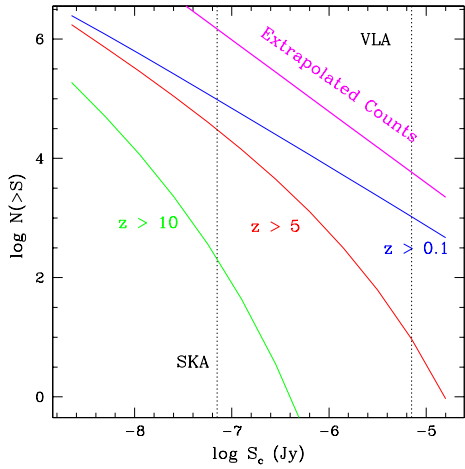


Figure 4. Number of sources which may be detected in the 1° by SKA, as a function of the threshold flux S_c . Realistic limiting fluxes for point source detection are shown. The extrapolated source counts from [36] are also shown. From [33].

at 2 GHz, corresponding to a free-free distortion parameter $y_B \simeq 1.5 \times 10^{-6}$, well within the observational capability of DIMEs [23,7].

6. CONCLUSION

Although not specifically devoted to CMB studies, because of its high resolution and the limited high frequency coverage, the extreme sensitivity and resolution of SKA may be fruitfully used for a detailed mapping of the thermal plasma properties in the intergalactic and intracluster medium and at galaxy scale.

On the basis of the existing literature, we discussed the SKA contribution to the understanding of some topics of relevant interest in cosmology, from the detailed mapping of the SZ effect towards cluster of galaxies, to the number counts and imaging possibilities of the SZ effect from early quasars and proto-galactic gas and of the

free-free emission from early ionized halos. We also discussed the contribution of SKA to the future CMB spectrum space experiments, devoted to the comprehension of the plasma thermal history at early epochs, through the extremely accurate control of extragalactic radio source counts at very faint fluxes.

A. SKA SENSITIVITY IN TERMS OF ANGULAR POWER SPECTRUM

The properties of a large population of astrophysical objects can be studied by exploiting the details of the sources in dedicated fields and by analyzing the field statistical properties.

The statistics of temperature anisotropy is typically analyzed in spherical harmonics $Y_{\ell m}$:

$$\frac{\delta T}{T}(\hat{\gamma}) = \sum_{\ell=1}^{\infty} \sum_{m=-\ell}^{\ell} a_{\ell m} Y_{\ell m}(\hat{\gamma}), \quad (21)$$

where $\hat{\gamma}$ is the observation unit direction vector. By assuming isotropy around the observer, $a_{\ell m}$ should have zero mean, $\langle a_{\ell m} \rangle = 0$, and variance C_{ℓ} ² given by:

$$C_{\ell} \equiv \langle |a_{\ell m}^2| \rangle = \frac{1}{2\ell+1} \sum_m a_{\ell m}^2. \quad (22)$$

The correlation function of the temperature anisotropy, $C(\theta) \equiv \langle \frac{\delta T}{T}(\hat{\gamma}_1) \frac{\delta T}{T}(\hat{\gamma}_2) \rangle$, is related to the angular power spectrum by the equation:

$$C(\theta) = \frac{1}{4\pi} \sum_l (2l+1) C_{\ell} P_{\ell}(\cos \theta); \quad (23)$$

here $\cos \theta = \hat{\gamma}_1 \cdot \hat{\gamma}_2$ and P_{ℓ} is the Legendre polynomial.

At SKA resolution and sensitivity the standard approaches to compute the angular power spectrum of anisotropies from classes of astrophysical

²Roughly speaking, a multipole $\sim \ell$ corresponds to an angular scale $\vartheta/\text{deg} = 180/\ell$. In this convention C_{ℓ} is dimensionless. It is also useful to bear in mind that the same expansion in spherical harmonics can be considered for the (physical) temperature fluctuation δT , instead of the dimensionless temperature fluctuation $\delta T/T$; in this case the physical dimension of C_{ℓ} will be the square of a temperature. Given the CMB monopole temperature of 2.725 K [29], the dimensionless C_{ℓ} will be $\simeq 7.4 \times 10^{12}$ smaller than the C_{ℓ} expressed in terms of μK^2 (in thermodynamic temperature).

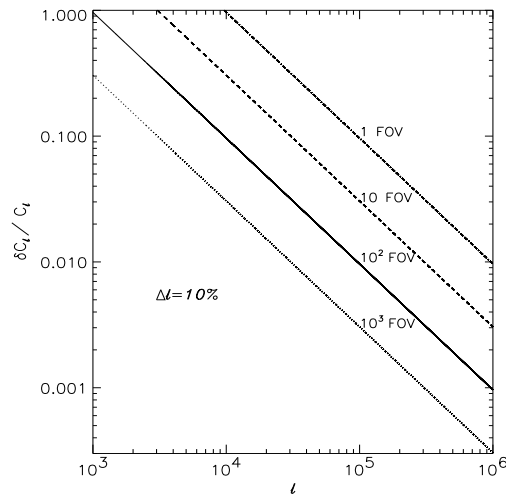


Figure 5. Relative uncertainty on CMB angular power spectrum recovery from combined cosmic and sampling variance for some representative sky coverages.

sources, typically based on the assumption that sources above the detection level do not significantly merge in the same image pixel, are no longer valid since the expected number of (no longer point-like) sources per resolution element may be large and the source diffuse emission extends over several (or many) image pixels (see, e.g., Fig. 2). Further studies are then necessary to characterize the correlation properties of source populations as observed at SKA resolution and sensitivity.

In spite of this uncertainty, it is important to characterize the nominal SKA capability to recover these kinds of statistical information.

We then “rewrite” here the typical SKA sensitivity in terms of accuracy in the recovery of the angular power spectrum.

Since each given anisotropy field is a single realization of a stochastic process, it may be different from the average over the ensemble of all possible realizations of the given (true) model with given parameters. This translates into the fact that the

$a_{\ell m}$ coefficients are random variables (possibly following a Gaussian distribution), at a given ℓ , and therefore their variance, C_ℓ , is χ^2 distributed with $2\ell + 1$ degrees of freedom. The relative variance δC_ℓ on C_ℓ is equal to $\sqrt{2/(2\ell + 1)}$ which is quite relevant at low ℓ because of the relatively small number of available modes. This is the so-called “cosmic variance” that defines the ultimate limit on the accuracy at which a given model defined by an appropriate set of parameters can be constrained by the angular power spectrum. Another similar variance in anisotropy experiments is related to the sky coverage since the detailed anisotropy statistical properties may depend on the considered sky patch. This variance depends on the observed sky fraction, f_{sky} . At the largest multipoles achievable with a given experiment the most relevant uncertainties are related to the experiment resolution and sensitivity. All these terms contribute to the final uncertainty on the angular power spectrum according to [22]:

$$\frac{\delta C_\ell}{C_\ell} = \sqrt{\frac{2}{f_{\text{sky}}(2\ell + 1)}} \left[1 + \frac{A\sigma^2}{NC_\ell W_\ell} \right], \quad (24)$$

where A is the size of the surveyed area, σ is the rms noise per pixel, N is the total number of observed pixel, and W_ℓ is the beam window function. For a symmetric Gaussian beam $W_\ell = \exp(-\ell(\ell + 1)\sigma_B^2)$ where $\sigma_B = \text{FWHM}/\sqrt{8\ln 2}$ defines the beam resolution. In the limit of an experiment with infinite sensitivity ($\sigma = 0$) $\delta C_\ell/C_\ell$ is determined only by cosmic and sampling variance; in this limit, by assuming also full sky coverage ($f_{\text{sky}} = 1$), $\delta C_\ell/C_\ell$ is determined only by the cosmic variance.

At $\simeq 20$ GHz a typical SKA field of view (FOV) is of $\simeq 4' \times 4'$ and a sky coverage of $\simeq 10^2$ FOV corresponds to about $\simeq 40' \times 40'$, possibly achievable with mosaicing techniques.

The relative error $\delta C_\ell/C_\ell$ due to cosmic and sampling variance is shown in Fig. 5 by considering a binning of $\simeq 10\%$ in ℓ which allows to reduce $\delta C_\ell/C_\ell$ by a factor $\sqrt{0.1\ell}$ and is not critical, being quite smooth the C_ℓ dependence on ℓ for the kinds of anisotropies considered in this work. As evident the sky coverage corresponding to $\sim 10^2$ SKA FOV (or to ~ 1 SKA FOV)

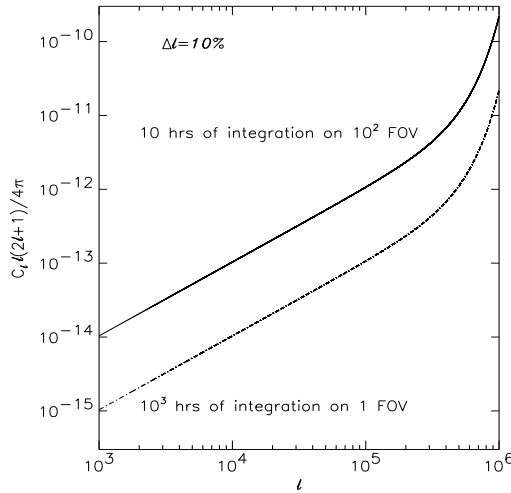


Figure 6. Absolute uncertainty on dimensionless CMB angular power spectrum recovery due to the instrumental noise for some reference cases (see also the text).

allows to reach a relative “fundamental” uncertainty less than $\simeq 10\%$ at $\ell \simeq 10^4$ (or at $\simeq 10^5$) and significantly smaller at larger multipoles.

The smallest angular scales (or the highest multipoles) achievable with a good accuracy are set by the instrument resolution and sensitivity.

By using about 50% of the collecting area ³ SKA would allow the mapping of diffuse anisotropies up to $\ell \sim 10^6$. We will use this case as a reference.

The absolute error δC_ℓ due to the instrumental noise is shown in Figs. 6 and 7, again by considering a binning of $\simeq 10\%$ in ℓ , respectively in terms of $C_\ell \ell(2\ell+1)/4\pi$ with dimensionless C_ℓ

³In this context, the whole SKA collecting area could represent a real improvement only provided that surface brightness (or temperature) anisotropy maps at higher resolution could be degraded at lower resolution to improve the rms (white noise) sensitivity per resolution element (according to the ratio of the corresponding FWHM) by averaging the brightness temperatures of the small pixels which constitute a larger pixel, a point that should be accurately verified through detailed simulations.

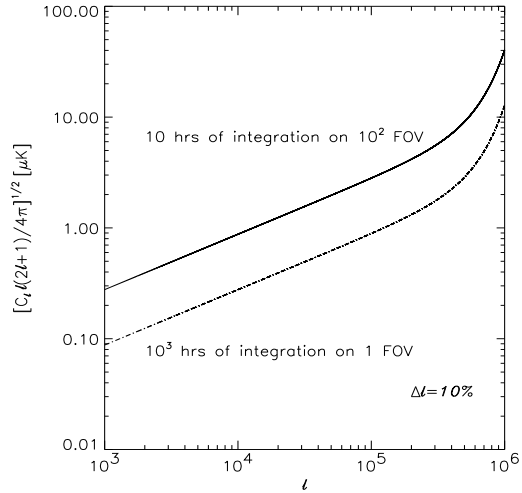


Figure 7. The same as in Fig. 6, but in terms of the temperature fluctuation $\sqrt{C_\ell \ell(2\ell+1)/4\pi}$.

and of $\sqrt{C_\ell \ell(2\ell+1)/4\pi}$ with C_ℓ in μK^2 (note that we do not refer here to the noise angular power spectrum but to the uncertainty on the signal angular power spectrum recovery, i.e. to the rms of “residual” noise angular power spectrum after the subtraction of its expectation value obtained on the basis of the accurate knowledge of the instrumental noise properties, as necessary in CMB anisotropy experiments).

ACKNOWLEDGMENTS It is a pleasure to thank A. Cavaliere, L. Danese, C. Fanti, F. Finelli, G.L. Granato, A. Lapi, N. Mandlesi, P. Platania, L.A. Popa, R. Salvaterra, and L. Silva for collaboration and discussions. The use of the CMBFAST code is acknowledged.

REFERENCES

1. Aghanim N., Bland C., Silk J., 2000, A&A, 357, 1
2. Barlett J.G., Stebbins A., 1991, ApJ, 371, 8

3. Bond J.R., Cole S., Efstathiou G., Kaiser N., 1991, *ApJ*, 379, 440
4. Bullock J.S., et al., 2001, *MNRAS*, 321, 559
5. Burigana C., Danese L., De Zotti G., 1991, *A&A*, 246, 59
6. Burigana C., Finelli F., Salvaterra R., Popa L.A., Mandolesi N., 2004, in *Recent Research Developments in Astronomy & Astrophysics* – Vol. 2, 59
7. Burigana C., Salvaterra R., 2003, *MNRAS*, 342, 543
8. Danese L., De Zotti G., 1980, *A&A*, 84, 364
9. Dawson K.S., et al., 2002, *ApJ*, 581, 86
10. De Zotti G., et al., 2004, in *Proc. Int. Symp. Plasmas in the Laboratory and in the Universe: new insights and new challenges*, Como, September 2003, eds. Bertin G., Farina D., Pozzoli R., pg. 375, *astro-ph/0401191*
11. da Silva A.C., et al., 2001, *ApJ*, 561, L15
12. Ferrarese L., 2002, in *Current high-energy emission around black holes*, eds. C.-H. Lee & H.-Y. Chang, Singapore: World Scientific Pub.
13. Fixsen D.J., et al., 1996, *ApJ*, 473, 576
14. D.J. Fixsen and J.C. Mather, 2002, *ApJ*, 581, 817
15. Gnedin N.Y., Jaffe A.H., 2001, *ApJ*, 551, 3
16. Granato G.L., et al., 2001, *MNRAS*, 324, 757
17. Haiman Z., Loeb A., 1998, *ApJ*, 503, 505
18. Hummer D.G., Storey P.J., 1987, *MNRAS*, 224, 801
19. Ikeuchi S., 1981, *PASJ*, 33, 211
20. Jones M.E., 2003, in *The scientific promise of the Square Kilometer Array*, SKA Workshop, Oxford, 7 November 2002, eds. Kramer M., Rawlings S., pg. 47, http://www.skatelescope.org/documents/Workshop_Oxford2002.pdf
21. Lapi A., Cavaliere A., De Zotti G., 2003, *ApJ*, 597, L93
22. Knox L., 1995, *Phys. Rev. D.*, 48, 3502
23. Kogut A., 1996, *Diffuse Microwave Emission Survey*, in XVI Moriond Astrophysics meeting *Microwave Background Anisotropies*, March 16-23, Les Arcs, France, *astro-ph/9607100*
24. Kogut A., 2003, in the Proc. of *The Cosmic Microwave Background and its Polarization*, New Astronomy Reviews, eds. Hanany S., Olive K.A., Vol. 47, Issues 11-12, p. 945
25. Kogut A., et al., 2003, *ApJS*, 148, 161
26. Ma C.-P., Fry J.N., 2002, *PRL*, 88, 211301
27. Mason B.S., et al., 2003, *ApJ*, 591, 540
28. J.C. Mather et al., 1990, *ApJ*, 354, L37
29. Mather J.C., Fixsen D.J., Shafer R.A., Mosier C., Wilkinson D.T., 1999, *ApJ*, 512, 511.
30. Natarajan P., Sigurdsson S., Silk, J., 1998, *MNRAS*, 298, 577
31. Natarajan P., Sigurdsson S., 1999, *MNRAS*, 302, 288
32. Navarro J.F., Frenk C.S., White S.D.M., 1997, *ApJ*, 490, 393
33. Oh S.P., 1999, *ApJ*, 527, 16
34. Oh S.P., Cooray A., Kamionkowski M., 2003, *MNRAS*, 342, L20
35. Ostriker J.P., Vishniac E.T., 1986, *ApJ*, 306, L51
36. Partridge R.B., Richards E.A., Fomalont E.B., Kllerman K.I., Windhorst R., 1997, *ApJ*, 483, 38
37. Pei Y., 1995, *ApJ*, 438, 623
38. Platahia P., Burigana C., De Zotti G., Lazzaro E., Bersanelli M., 2002, *MNRAS*, 337, 242
39. Prandoni I., et al., 2001, *A&A*, 365, 392
40. Press W.H., Schechter P., 1974, *ApJ*, 187, 452
41. Rees M.J., Ostriker J.P., 1977, *MNRAS*, 179, 541
42. Rephaeli Y., 1995, *ARA&A*, 33, 541
43. Rybicki G.B., Lightman A.P., 1979, *Radiative Processes in Astrophysics*, Wiley, New York
44. Salvaterra R., Burigana C., 2002, *MNRAS*, 336, 592
45. Springel V., White M., Hernquist L., 2001, *ApJ*, 549, 681
46. Sasaki S., 1994, *PASJ*, 46, 427
47. Silk J., 1968, *ApJ*, 151, 459
48. Stebbins A., Silk J., 1986, *ApJ*, 169, 1
49. Subrahmanyan R., Ekers R.D., 2002, in the XXVIIth General Assembly of the URSI, August 17-24, Maastricht, The Netherlands, *astro-ph/0209569*
50. Sunyaev R.A., Zeldovich Ya.B., 1970, *Ap&SS*, 7, 20
51. Sunyaev R.A., Zeldovich Ya.B., 1972, *Comm.*

Astrophys. Space Phys., 4, 173

- 52. Toffolatti L., et al., MNRAS, 1998, 297, 117
- 53. Tremaine S., et al., 2002, ApJ, 574, 740
- 54. Vishniac E.T., 1987, ApJ, 322, 597
- 55. White S.D.M., Rees M.J., 1978, MNRAS, 183, 341
- 56. Zeldovich Ya.B., Sunyaev R.A., 1969, Ap&SS, 4, 301